Intense rains in Israel associated with the 'Train effect'

Baruch Ziv[1], Uri Dayan[2], Lidia Shendrik[1], Elyakom Vadislavsky[3]

[1] Department of Natural Sciences, The Open University of Israel, Raanana, Israel

5   [2] Department of Geography, The Hebrew University of Jerusalem, Jerusalem, 9070227, Israel

[3] The Israeli Meteorological Service (IMS), Beit Dagan, Israel

Correspondence: Baruch Ziv (zivbaruchana@gmail.com)

Abstract. 'Train effect' is defined as a cloud system in which several convective cells pass over the same place

10   in a short time. Trains produce large amount of rainfall, frequently leading to flash floods, reported mainly over North America during spring and summer. Thirty train events were identified, using radar images, calibrated by rain-gauges, for four winters, all associated with Cyprus Lows (CL). The dynamic factors responsible for their formation in Israel were examined, utilizing the ECMWF Integrated Forecast System of 0.1° resolution.

15   Seventeen out of the 30 events share common features. Each one was found at the cold sector in the southern periphery of a CL at its occluded stage, and located in the left flank of a maximum wind belt, where cyclonic shear vorticity exists. The trains cross the Israeli coast near 32.2°N, with a mean length of 35 km, last 2-3 hours, and yield a total of 30-50 mm rainfall. The maximum wind belts right of the trains were found to delineate the limit of the precipitative region of the CLs. Unlike classical trains, activated by thermal or frontal

20   forcing, the East Mediterranean trains that develop in cold air-mass, can be entitled 'cold trains', rather than the classical 'warm trains'.

1 Introduction

25   The Mediterranean Lows that reach its eastern part are called Cyprus Lows (CLs). These are mid-latitude cyclones (HMSO 1962; Ulbrich et al., 2012) that are responsible for about 90% of the annual rainfall in Israel (Goldreich et al., 2004). The daily rainfall associated with CLs is in the order of 10 – 30 mm (Striem 1981; Saaroni et al., 2010), and the extreme values exceed 50 mm (Katsnelson, 1964; Sandler et al., 2024), sometimes within a couple of hours (Morin et al., 2007, Dayan et al., 2021). Hereafter, 'rainfall' refers to the total amount

30   (mm) over a certain period and time, and 'rain rate' is expressed in mm h^{-1} units.

Cell propagation vector, called also "the train effect", refers to intense rains, "where cells form and pass repeatedly, in succession, over the same location, results from a linear organization" (Doswell et al., 1996). The cloud elements composing the typical train belong to the family of meso-scale convective complexes (MCC). The train is a meso-scale phenomenon, supported by synoptic scale processes, mostly through

35   "moistening and destabilization created by the modest but persistent synoptic-scale vertical ascent ahead of short-wave troughs" (Doswell, 1987). Actually, the synoptic- and the meso-scale factors interact synergistically to form the lower-level convergence accompanied by upper-level divergence conditions that last for several hours (Chappell, 1986). Intensive meso-scale uplift alone is insufficient to activate the train

without the support of the moderate uplift imparted by the synoptic factor. The mesoscale factor may be indiscernible but can be deduced from the inability of the synoptic ingredients alone to explain heavy precipitation associated with a train (Doswell et al., 1996).

The train effect is associated with quasi-stationary cold fronts or within pre-frontal warm tongues, mainly during the spring and summer (Chappell, 1986; Doswell et al., 1996). It has been reported mostly over North America (Schwartz et al., 1990; Corfidi, 2003; Wang and Chen 2009). An essential factor for maintaining a train is a continuing transport of moist and unstable air. An effective system that supplies such a transport is the low-level jet (LLJ) that tends to form near cold fronts (Wang and Chen 2009).

Train effect was identified also in Western Europe. Rigo and Llasat (2005) analyzed a "convective train", associated with a meso-scale cyclone that produced a summer severe flash flood in southeastern Spain. ZAMG (2014) analyzed 100 convective systems over the Iberian Peninsula and France during the period 1992 - 2009, 7 of them in the form of trains, with lengths of hundreds of kilometers, all ahead of a cold front (i.e., pre-frontal train). One of them lasted for 16 hours. As major conditions for train generation, they mentioned LLJ near 925 hPa and convergence of specific humidity at 1000 hPa.

Heavy rains associated with cloud strips resembling the train effect have been identified in the East Mediterranean (EM). The cloud elements composing these systems were not in the form of MCC, but rather smaller or less persistent cells. These cloud systems were analyzed first by Rosenfeld and Nirel (1996), who considered them as 'coastal fronts' (e.g., Bosart 1975), which are formed by convergence of land breezes. Rosenfeld and Nirel (1996) attributed these systems to convergence between a southerly land-breeze originating from the North African and North Sinai Desert coasts and the westerlies associated with a CL over the adjacent Mediterranean (Fig. 1). When such a cloud strip crosses the Israeli coastline, it might generate continuous rain. Goldreich et al. (2004) stated that the rain produced by this type of coastal fronts lasts 20 hours on the average and that they are most frequent in December, when the sea-land temperature contrast is the largest, and most active during the night and early morning hours.
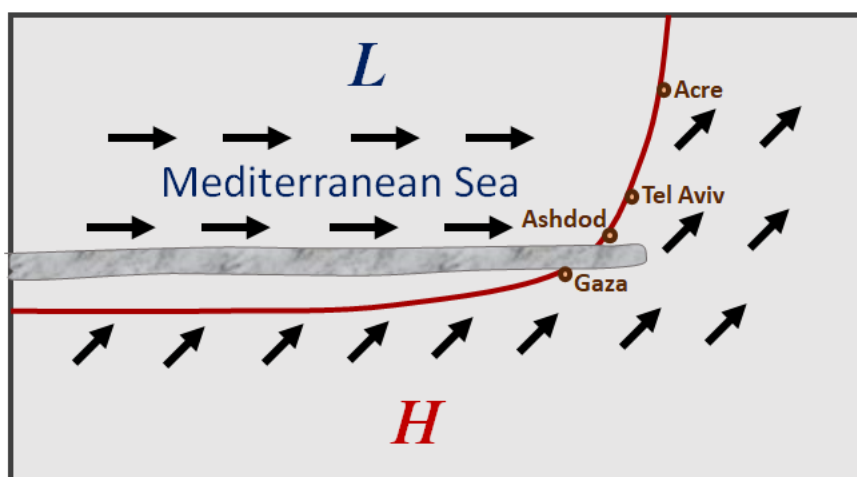

Figure 1. A Schematic illustration of cloud-strips producing rain over the southern coast of Israel. L and H denote cyclone and anticyclone, respectively, the arrows represent wind vectors and the shading – the cloud strip (following Fig. 6 of Rosenfeld and Nirel 1996)

The first time in which the term "train" was attributed to a rain system in Israel was by Dayan et al. (2021). They analyzed a severe flash flood that was generated by a series of consecutive convective rain cells within less than 2 hours in south Israel, within the cold sector of a CL in April 2018. The flash flood took place in Tzafit Creek, in south Israel (31.0°N, 35.3°E) and took the lives of 10 people. This case demonstrates the fatal potential of such a phenomenon for this region. It is worth noting that this train, and these analyzed in the present study, were found within the cold sector of mid-latitude cyclones, unlike the trains analyzed in North America and Europe, which were found within warm air masses and can not be explained by the same mechanisms. We entitle them 'cold trains', in contrast with the 'warm trains' previously studied.

The aim of this research is to identify and document trains that are associated with CLs, and to analyze the major dynamic factors responsible for their formation. Section 2 specifies the data and methods used. Section 3 demonstrates the phenomenon by a case study and attempts to generalize its characteristics through composite maps. In the last section the results are discussed and summarized in a framework of a conceptual model.

2 Data and Methods

The study relies on four consecutive winters (December-February) of the years 2018 -2022 (except January-February 2019 due to missing radar data), a total of 10 months, when CLs are most frequent (Alpert et al., 2004). The rain data are based on the radar of the Israeli Meteorological Service (IMS), calibrated by rain gauges, using the INCA system integration method (Haiden et al., 2011), operated by the IMS.

The synoptic background as well as the meso-scale features for the cases analyzed are based on the atmospheric fields of the gridded data of the European Centre for Medium-Range Weather Forecasts (ECMWF) Integrated Forecast System (IFS) of 0.1° resolution (Hólm et al., 2016). This includes the sea-level pressure (SLP) and 3 wind components from all levels between 925 and 200 hPa. This data set was found superior over the ERA5 in resolving the signature of the trains in the rain field as well as in the vertical velocity field.

The train events were identified through inspection of the radar images for the rainy days included in the study period, in which CLs dominated the Levant region. An example is shown in Fig 2, and the location of the CL is denoted in Figs 1 and 2b. We used images, with a 5-min increments, searching for repetitive passages of cloud cells, producing instantaneous rain intensity of >30 mm h^{-1}, during 1 hour or more. These are regarded as 'train events', or 'events', hereafter. In such a way, 30 events were identified, and for each of them an integrated rainfall map was extracted.

Compositing of atmospheric fields enables combining information from a number of examples of a phenomenon in a convenient format that highlights basic common features, while eliminating detail of individual events (Sinclair and Revell, 2000). The individual maps were transformed to bring them to a common basis, so that in each one the cyclone center would be north of the train center, 500 Km apart. This transformation includes rotation, translation and scale changing. The first step was to rotate each map about the location of the cyclone's center (which served as a 'reference point') by an angle equal (and opposite) to the deviation of the orientation of the line connecting the centers to the train and the cyclone from the south-north

3

direction. The second step was to rotate the wind direction accordingly in every grid point. The third was to stretch (or contract) the grid to bring the distance between the centers of the train and the cyclone to 500 Km. The locations of the CLs' centers were identified as the minimum in the 925 hPa geopotential height (GPH) closest to Cyprus. If such a minimum was not found, the nearest cyclonic vortex at that level was regarded as the CL center. The details of the variables for which composite maps were derived and the specific transformations used are specified in the "results" section.

3 Results

In attempting to identify the mechanisms responsible for train events, we isolated from the 30 train events 17 that had a common feature. All of them were found to delineate the southern boundary of the rainy sector within the cold sector of CLs, in the vicinity of band of maximum wind. These 17 trains were separated from the other 13 trains, which were not attributable to any other common one, and constitute the 'study sample'. First, they are exemplified by a case study, and then analyzed collectively by composite maps.

3.1 A case study

During 6 - 8 December 2018 the EM was dominated by a CL (Fig. 2a), accompanied by an upper-level trough, which axis was located to the east of the Levant (Fig. 2c). Rains were spread over the northern half of Israel, the region characterized by Mediterranean climate type denoted 'Cs' according to Koeppen classification, i.e., "The thermal zones of the earth according to the duration of hot, moderate and cold periods and to the impact of heat on the organic world" (Volken and Brönnimann. 2011). The rainiest area was the coastal plain, with 200-270 mm rainfall, and the Judean Mountains, extending east of it (including Jerusalem) that received half of this amount (IMS publication, 2018).

On December 7th the center of the CL was located at the northeastern corner of the Mediterranean, as can be inferred by a vortex in the 925 hPa level there (Fig. 2b). The rainfall during that day over the northern half of Israel was 30-40 mm, with a few peaks of ~60 mm over the coastal plain. On that day, at 19:30 UTC, a cloud strip in a form of a train, oriented in a west-east direction, developed across the central part of the coastline (Tel Aviv, 32.2°N Fig. 3). This system persisted 2.5 hours and generated heavy rain, with a maximum instantaneous rate of over 60 mm h^{-1} (as inferred from Fig. 3a-e), summing up to >50 mm rainfall during the entire event (Fig. 2a). Another train occurred over the region in the previous day (Table 1, No. 1) and yielded an average rainfall of 50 mm (not shown). This implies that the two trains contributed ~35% of the total rainfall obtained over the coastal plain during the 3 days of the rainstorm. The train was 100 Km long, ~5 Km wide in its western end and > 10 Km in the eastern one (Fig. 3). It was composed of three cells, on the order of < 10 Km, two of them are shown in Fig. 3a-e (denoted *'A'* and *'B'*).
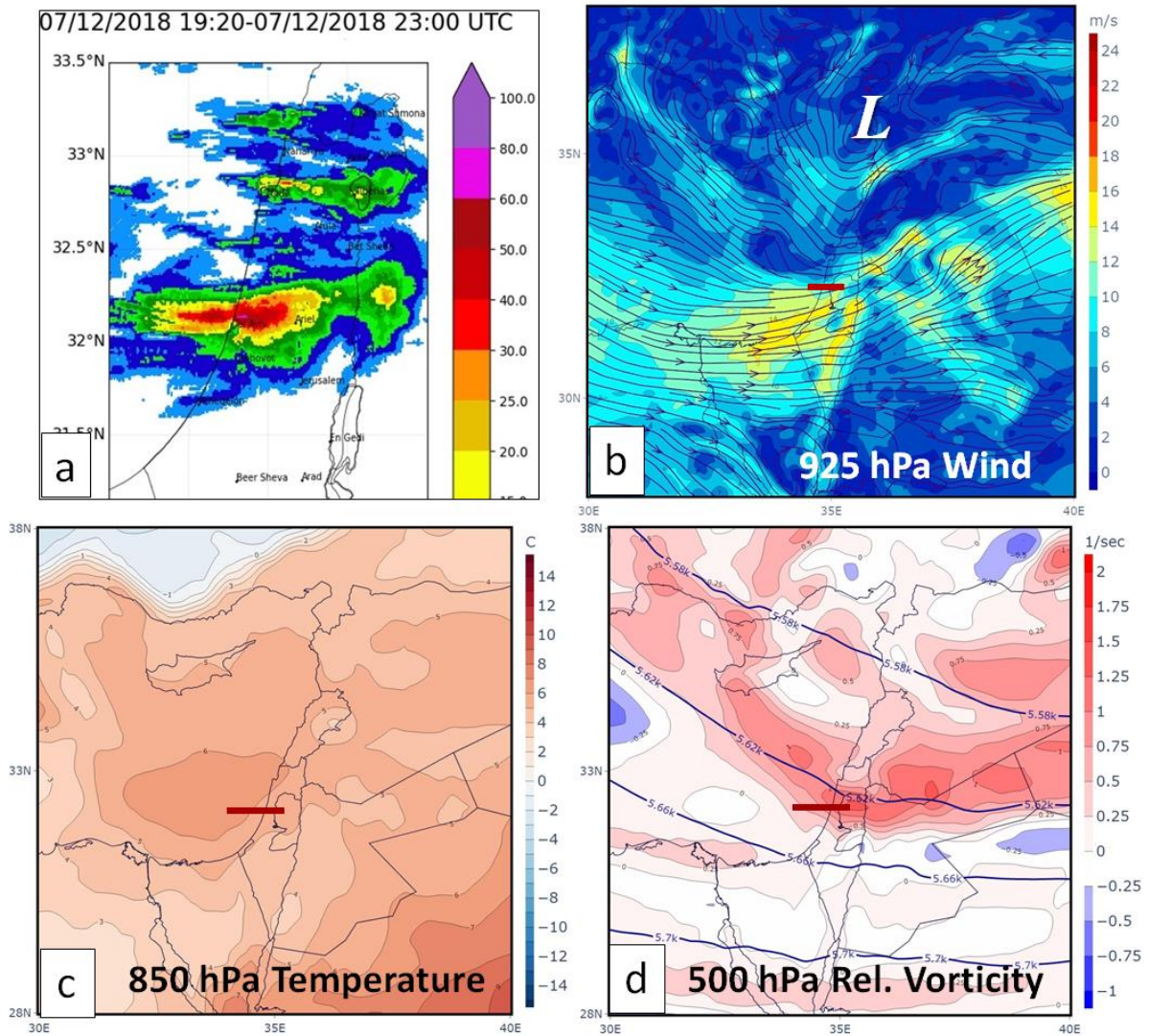
Figure 2. Synoptic conditions on 7 December 2018 of (a) Integrated rainfall during 1920-2300 UTC. Atmospheric fields are from 21:00 UTC: (b) Wind field (streamlines and speed, in ms⁻¹ units) at 925 hPa, (c). Temperature (°C) at 850 hPa and (d). Geopotential height (GPH, m) and relative vorticity (10⁻⁵ s⁻¹) at 500 hPa. The maps are derived from ECMWF Integrated Forecast System (IFS) of 0.1° resolution. The train is denoted by a red thick line

The lower level (925 hPa) wind field (Fig. 2b) shows that the EM and the Levant were under westerly flow, with cyclonic curvature and speed on the order of 5-10 ms⁻¹, except for a belt of ~15 ms⁻¹ over the southeastern Mediterranean. Confluence of the streamlines to the left of this belt is co-located with the train. The wind deviated 30° left of both the train orientation (Fig. 2b) and the tracks of the cloud cells (Fig. 3a-e). On the other hand, the isohypses at the 500-hPa (Fig. 2d) indicate that at that level the wind deviated 30° right of the train. This suggests that the clouds were stirred by the wind at the mid-troposphere. The lower-level temperature field (850 hPa, Fig. 2c) does not reflect any frontal structure, and indicates that this train was developed within a homogeneous air-mass, to the south of the CL center. This, and the absence of upper-level vorticity advection (Fig. 2d), indicate that the CL was at its occluded phase.
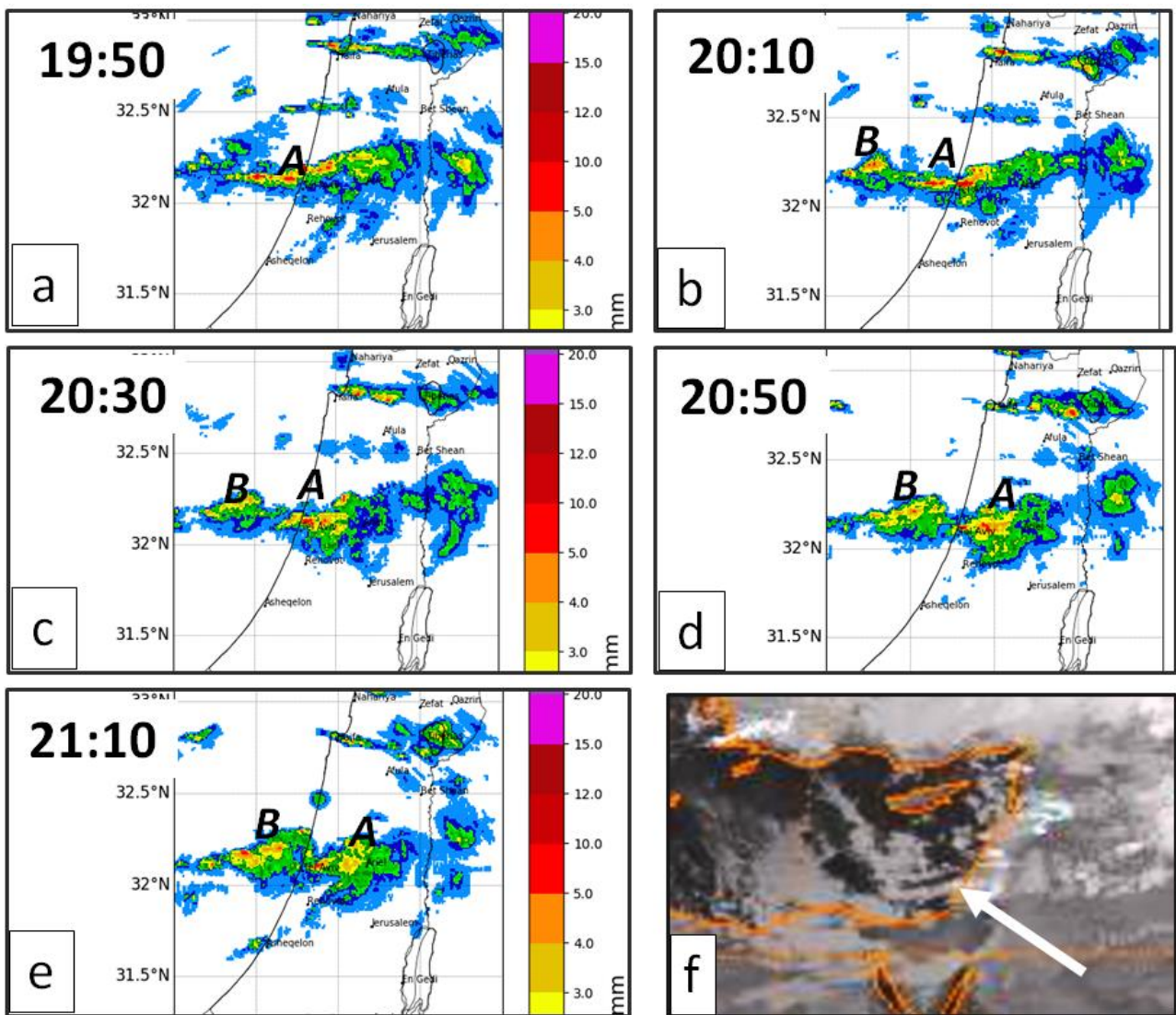
Figure 3. Cloudiness for 7 December 2018 (a-e). Radar imageries, at 19:50, 20:10, 20:30, 20:50 and 21:10 UTC, respectively, transformed to rain intensity (mm/10 min), the notations 'A' and 'B' refer to the 1st and 2nd rain cells, both advancing eastward in tandem. f. METEOSAT 8 IR imagery for 21:12 UTC. The white arrow points at the train location.

3.2 Common characteristics of the trains

The common features of the 17 trains included in the study sample are demonstrated through composite maps and specified in Table 1. The train events lasted between 1.3 and 5.1 hours, with an average of 2.3 hours, with no preferred time of the day for their occurrence. The average length of the trains was 44 Km, 5 of them were > 60 Km (maximum 100 Km) and 8 less than 30 Km. The mean latitude where the trains crossed the coastal region of Israel is near 32.2°N, with a tendency to be concentrated on its southern two thirds. Their centers were located at the coastline, within 0.5°, around 34.8°E, suggesting that the coast plays a role in their evolution. A significant relation was found between the orientation and the latitude of the trains. The trains affected the northern part of the coastline were oriented around 240-060°, while at the southern part their orientation was around 285-105°. A positive relation of 0.41, confident at the 0.10 Level. was found also

6

between the longitude of the cyclone center and the train orientation, i.e., trains associated with CLs east of the Mediterranean coast tended to be oriented northwest-southeast while those associated with CLs to the west, are oriented southwest-northeast. The maximum rainfall was between 20 and 70 mm, with an average of 35.5 mm. In 5 out of the 17 cases the values exceeded 50 mm, an amount which implies a high potential for flash flood in urban regions (e.g., Young, 2021). A substantial difference in precipitation activity was noted between the two sides of the train. In 13 of the 17 events, no rain was observed to the right (south) of the train. Also, in the remaining four events, the rain activity south of the train was much weaker than to the north of it.

Table 1. Selected features of the trains included in the study sample

No.	Date	Starting hour (UTC)	Duration (hours)	Lat of train (°N)	Length (Km)	Orientation (°)	Cyc center Lon (°E)	Cyc center Lat (°N)	Maximum rainfall (mm)*
1	07/12/2018	19:20	2.7	32.2	100	265	35.7	35.5	60
2	08/12/2018	03:00	2.5	31.7	20	270	35.4	36.2	60
3	05/12/2019	11:10	1.3	32.4	30	285	37.5	36.7	35
4	13/12/2019	13:30	2.0	32.9	30	240	36	36	45
5	13/12/2019	15:40	1.3	32.8	25	240	36	36	50
6	04/01/2020	02:00	2.5	32.6	65	240	34.1	34.5	45
7	04/01/2020	08:10	2.2	32.1	15	275	35	35.8	70
8	04/01/2020	11:30	1.0	31.7	20	280	35.1	36.3	35
9	05/01/2020	07:30	1.7	32.6	30	270	33.8	36	35
10	05/01/2020	11:00	4.0	32.6	100	270	35.8	35.5	55
11	08/01/2020	22:50	2.7	31.7	45	285	35	34.6	35
12	21/01/2020	19:10	2.2	32.0	20	350	36.5	33.5	35
13	18/12/2021	11:10	5.1	32.9	100	240	31	35.5	60
14	20/12/2021	19:40	2.3	31.9	85	285	35.5	36	28
16	16/01/2022	02:40	1.5	31.8	15	270	36	33.7	20
15	16/01/2022	05:50	2.2	31.7	20	270	36	33.7	45
17	26/01/2022	21:40	2.0	31.7	25	270	36.5	36	35
AVERAGE			2.3±1.0	32.2±0.5	44±32.4	271±26	35.3±1.4	35.4±1.0	35.5±13.5

* The maximum rate (calculated in 5 min intervals) with respect to the duration of the event over the affected area

Figure 4 shows the synoptic configuration under which the trains developed. The 500 hPa wind field (Fig. 4a) indicates the presence of an upper-level trough, slightly west of the CL, with a nearly westerly wind direction. This direction corresponds to that of the train and the movement of the individual cloud cells composing it (see Sec. 3.1 above). The lower-level wind field (Fig. 4b) demonstrates the criterion according to which the study sample was selected, i.e., a strip of maximum wind just to the right of the train. At the medium and higher-levels, as exemplified by the 500 hPa wind field (Fig. 4a), such a linkage can not be noted. This implies that the mechanism responsible for the train formation is found within the lower-levels, see discussion below. The 850 hPa temperature (Fig. 4c) shows a homogeneous temperature over the EM, around 3°C, which is bellow the long-term mean for each of the months included in the study period. It should be noted that similar homogeneity was seen in each of 16 out of the 17 cases, as exemplified in Fig. 2b. This eliminates the possibility that the trains were activated by fronts or warm air masses (see introductory Section 1, above).
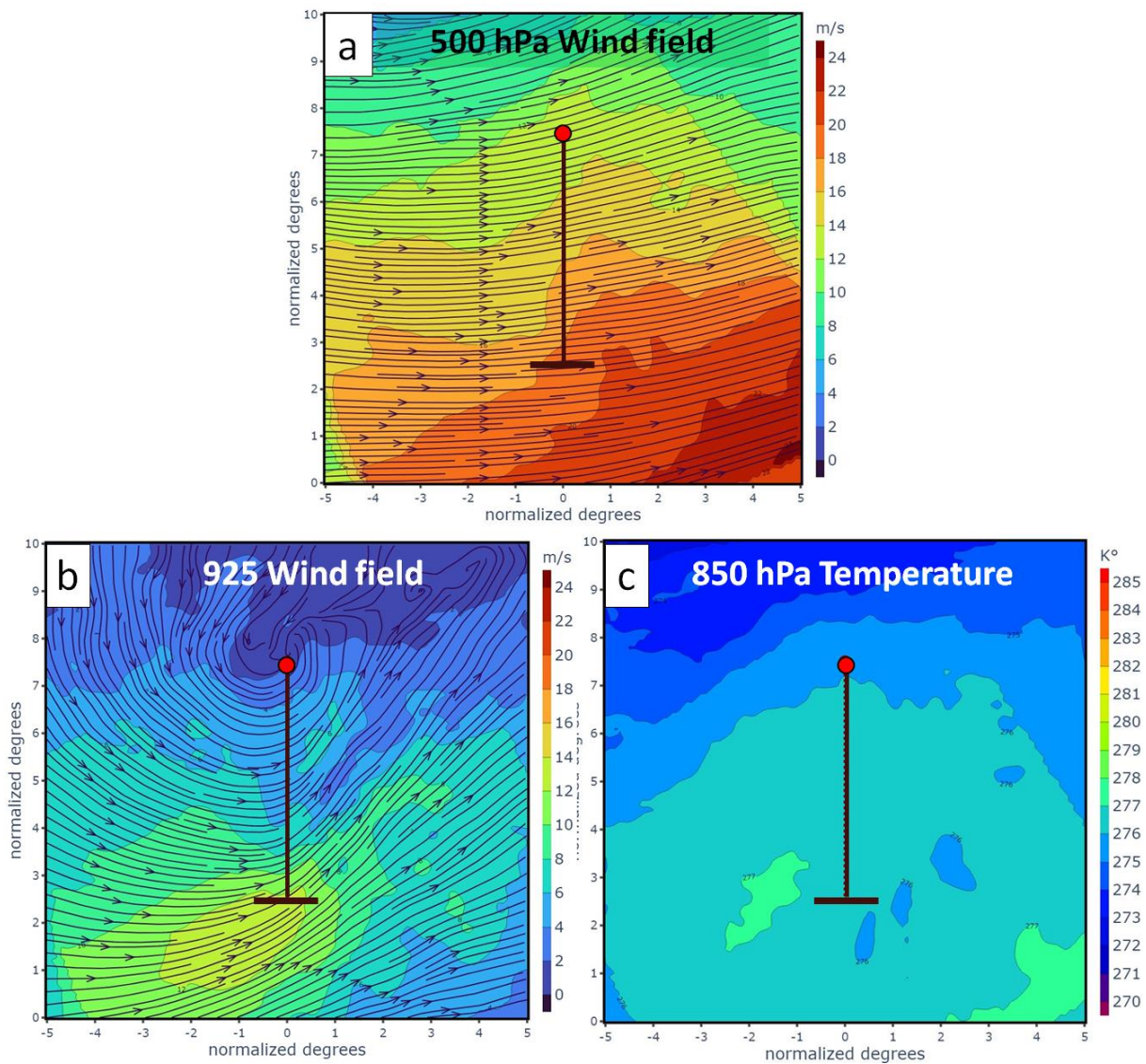

Figure 4. Composite map of the 17 members of the study sample: (a) and (b) wind field (streamlines and coloring according to wind speed, in ms⁻¹) in 500 and 925 hPa, respectively. (c). Temperature (°C) in 850 hPa. All individual maps are rotated, translated and rescaled to bring the cyclone center and the train to the same location. In each map the train is denoted by a horizontal red bar and the cyclone by a small red circle, with a thick line joining them.

205   Figure 5 presents the wind field with which the trains are associated. Figure 5a emphasizes the location of the train to the left of the maximum wind belt (see also Fig. 4b), where cyclonic shear vorticity exists. The positive vorticity to the left of this belt (elongated red band in Fig. 5b), stands in contrast with the negligible vorticity to its right. The absence of negative relative vorticity there can be explained by a cancellation of the negative

210   shear vorticity by a positive curvature vorticity imparted by the CL all over the region. The vertical meridional cross-section through the western part of the train, where the cloud cells evolve (Fig. 5c), shows a distinct ascending current, with a maximum of 10-20 cms^{-1} (rather large in meso-scale terms) between 800 and 700 hPa levels. The linkage between this updraft and the lower-level positive vorticity is elaborated in the following section.

215
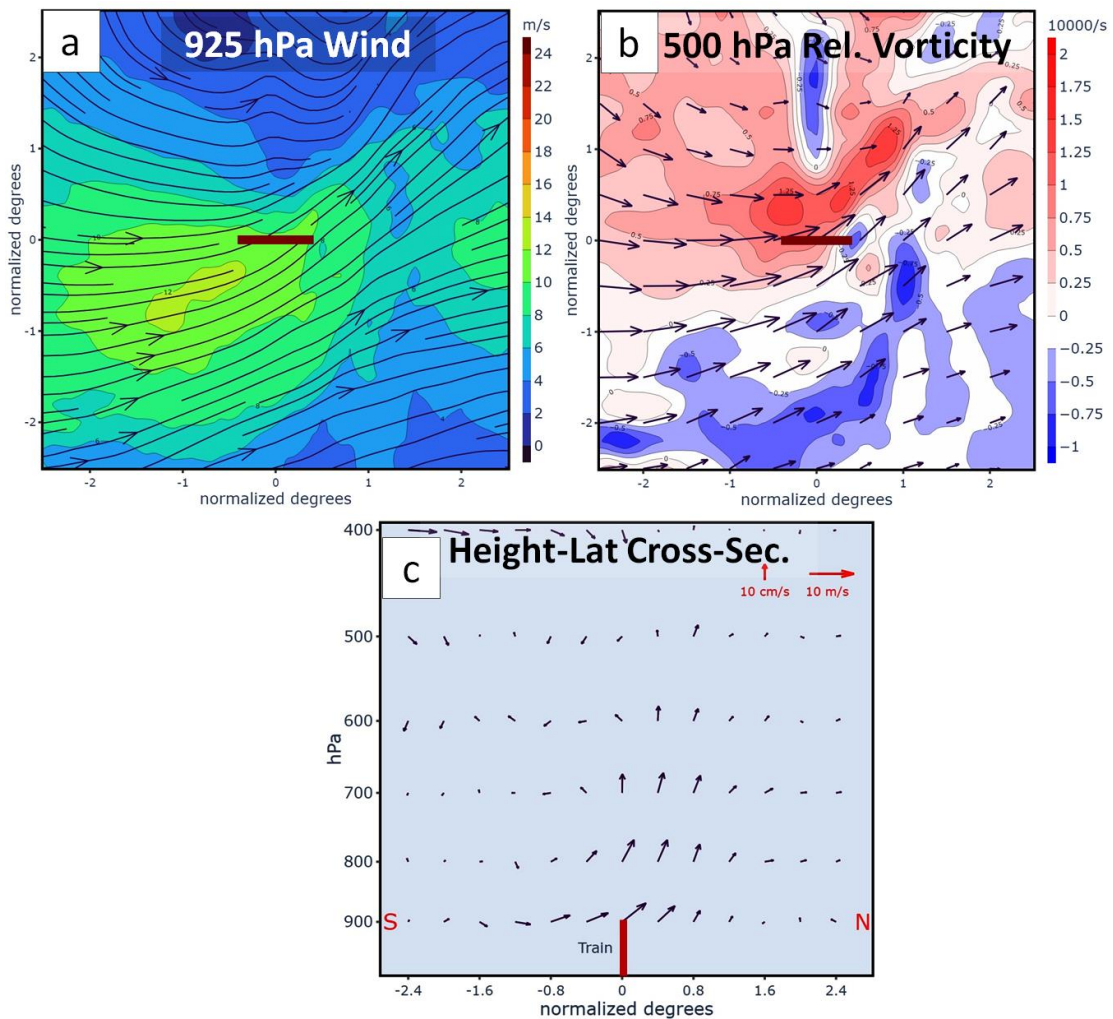
Figure 5. **(a-b): composite maps, but based on rotation and translation only, so as to bring the train to a zonal orientation: (a) wind speed and direction at 925 hPa. (b) wind and relative vorticity (s-1) at 500 hPa. The coordinates are degrees relative to train center. (c) vertical-meridional cross-section 10 Km**

220   **west of trains' centers of the meridional and vertical wind components. The x coordinates denote the latitude relative to the train, denoted by a thick red segment. The y coordinates is pressure, in hPa.**

9
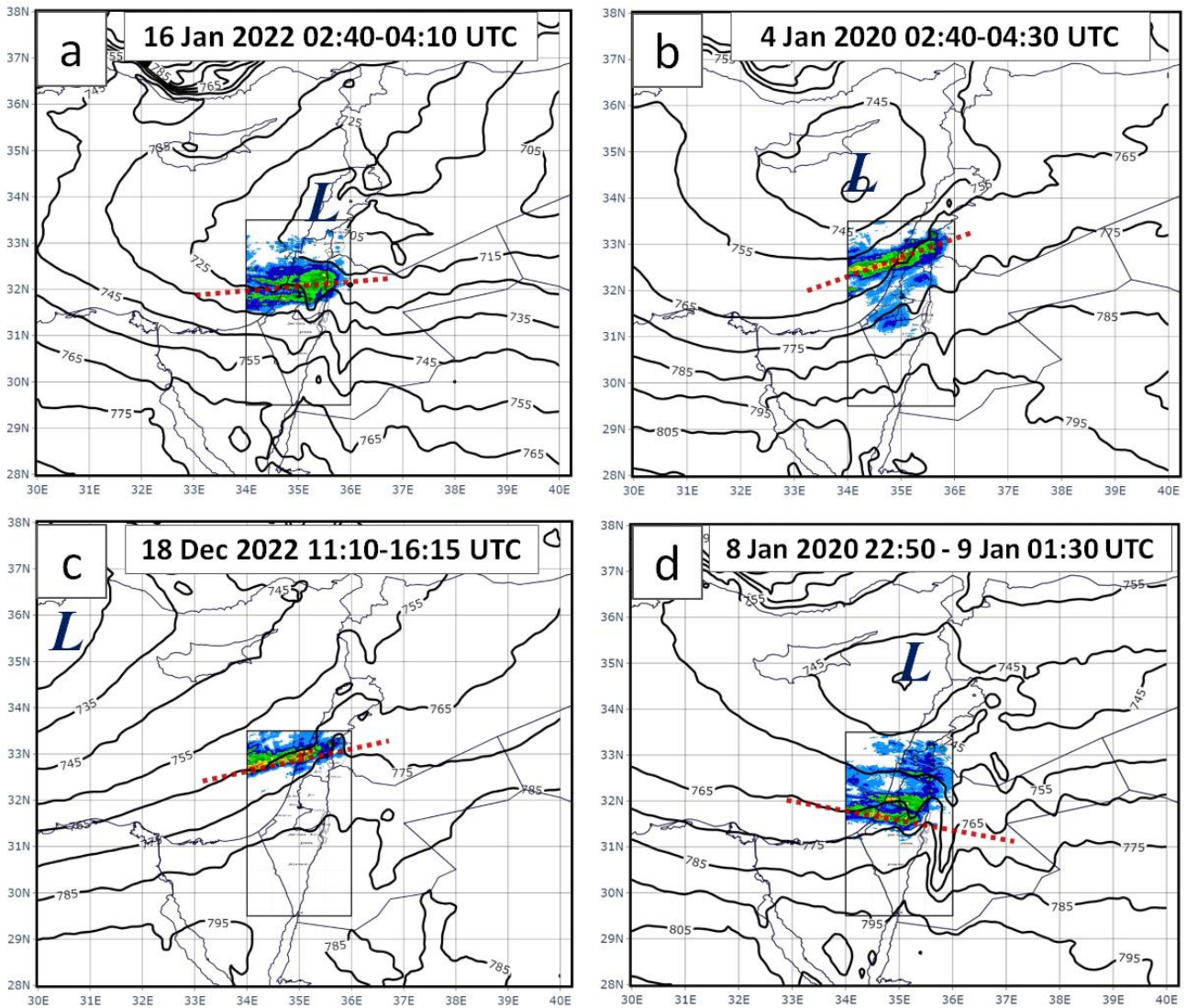
Fig. 6. Integrated rainfall superimposed on geopotential height for (a) 16 January 2022 02:40 - 04:10 UTC, (b) 4 January 2020 02:40 - 04:30 UTC, (c) 18 December 2022 11:10-16:15 UTC and (d) 8 January 2020 22:50 – 9 January 2020 01:30 UTC. In each panel, the rectangles encircling the rain maps denotes the radar coverage, the letter *L* denotes the cyclone center and the dotted red line – the location and orientation of the train. Note that only in panel "b" there was some rain south of the train.

4. Dynamical considerations

Analysis of 17 rain systems identified in the Levant, which meet the definition of the train effect, enabled us to characterize their main features. A dynamical framework for the cold train is proposed as follows: It develops along the left flank of a maximum wind belt, where cyclonic shear vorticity exists, along the southern periphery of a CL (Figs. 2b, 4b and 5a). They can be explained by an updraft (Fig. 5c) generated by a combination of cyclonic wind shear at the lower-level and surface friction. The mechanism is demonstrated schematically by Fig. 7. If no friction exists, and the region is subjected to south to north pressure drop, the pressure gradient, which is purely meridional (Fig. 7a), produces non-divergent geostrophic westerly winds. The magnitude of the pressure gradient attains a maximum in the middle of the domain, yielding a belt of maximum wind across the domain.
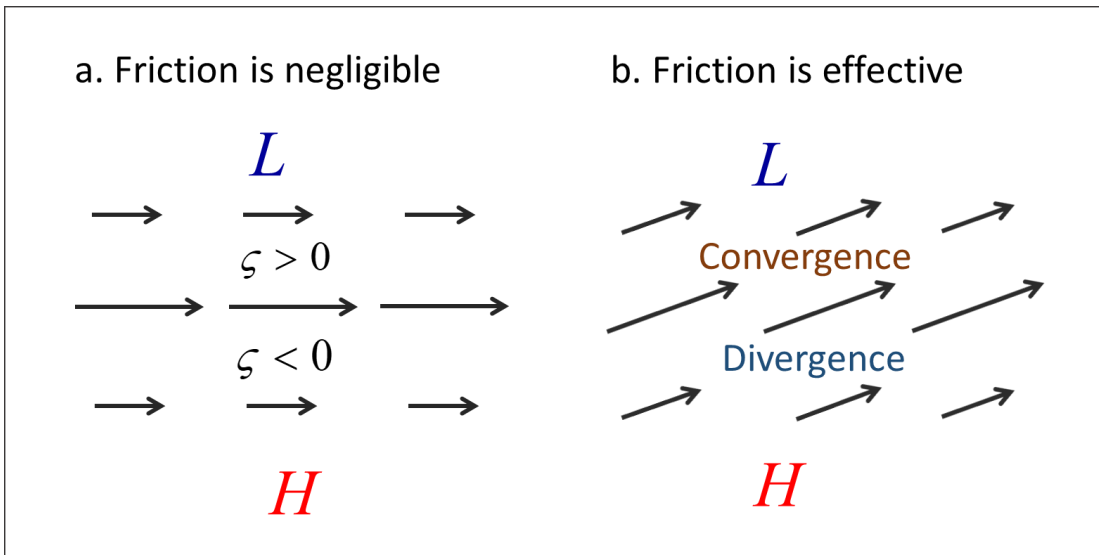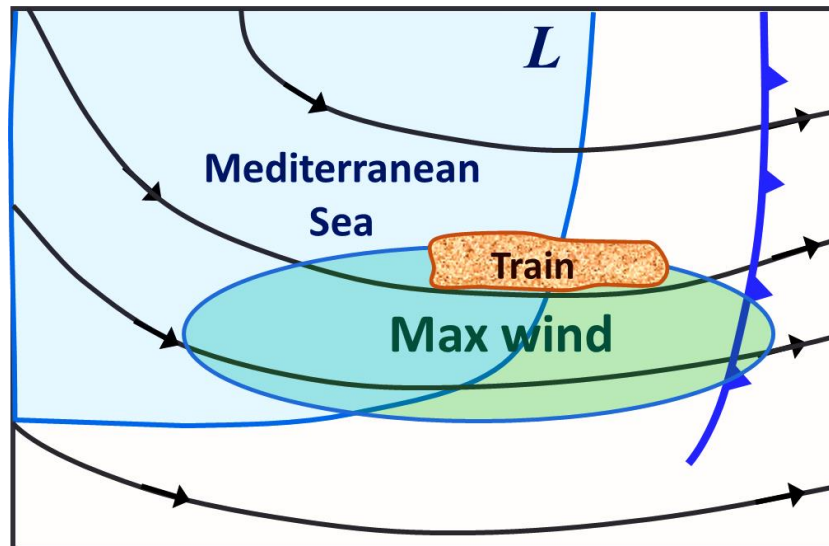
Figure 7. Schematic description of the wind pattern associated with zonally uniform south to north pressure gradient producing a band of maximum wind: (a) when friction does not exist, (b) when friction is imposed, and the wind speed is reduced by 30% and its direction is deflected by 30°.

When friction is imposed, under the same pressure field, the wind weakens and deviates to the left from its westerly direction (Fig. 7b). As a result, the weaker winds right of the maximum wind band blow toward the faster winds along the core of maximum wind, and the fast winds at the maximum wind belt blow toward the weaker winds to the left of the core. The result is a band of along-stream convergence left of the core of maximum wind and divergence to its right. The elongated convergence band to the left of the maximum wind provides the uplift required for train formation.

The co-existence of lower-level positive vorticity, the upward motion and the resulting train indicate that friction is effective over the sea surface where the trains are created. It should be noted that in most of the events the core of the maximum wind belt delineated the southern boundary of the active sector of the CL, in terms of cloudiness and precipitation. This type of trains reflects an interlace between the synoptic scale (the CL) with the meso-scale (the maximum wind belt), in accordance with Chappell (1986) and Doswell (1987, 1996). Both contribute to the updraft that produces this rain system, and the meso-scale factor determines its location and orientation.

The friction exerted by the sea surface seems questionable. Indeed, during calm conditions smooth sea surface produce negligible friction. But, under the influence of a CL, with its induced winds, waves are created, which may enhance friction. Wave height measurements at the Israeli coast at the days belonging to the study sample were taken from the "Coastal and Marine Engineering Research Institute Ltd (CAMERI)" in Israel (https://www.cameri-eng.com/). They show an average significant height of 2.41±0.61 meters, with an average maximum of 3.22±0.67 meters. This implies sea state 'rough', suggesting that friction cannot be ignored. Moreover, the presence of cumulus clouds associated with the CL creates turbulence that contributes friction as well. The combination of the factors that generate the trains is presented schematically in Fig. 8.

Figure 8. Schematic description of the lower-level configuration of the train associated with Cyprus Lows. The background covers the eastern part of the Mediterranean, the Levant and the coastal region of Sinai Desert. The black lines represent isobars and the arrowheads – the direction of the geostrophic wind. The blue 'L' denotes the CL center and thick line with the tooth represents the cold front. The region of the maximum wind within the lower 1 Km and the train itself are denoted.

5. Summary and discussion

The trains associated with CLs, analyzed above, are of meso-scale dimensions, i.e., ~35 Km long, 10-20 Km wide, persisting 2 - 3 hours and yielding 30-50 mm rainfall. They were entitled 'cold trains' since they were located within the cold sector of mid-latitude cyclones. They were found mainly in the winter, December – February, though such an event was documented in the spring (see section 1).

The cold trains and the "classical" warm trains share a common feature, i.e., lower-level uplift, which initiates deep convection under preexisting static stability. However, they differ in several aspects. The major difference between them is in the identity of the factor initiating their formation. For the trains associated with fronts, the factor is buoyancy, due to temperature difference across the front, whereas for the cold trains it is forcing exerted by lower-level convergence. Another difference is in their seasonality. While the 'warm trains' are formed in the spring and summer in North America (Doswell et al., 1996) and in Western Europe (e.g., ZAMG 2014), the trains in the EM are frequent mainly in the winter, when CLs prevail. The two types of trains differ also in their dimensions. The typical classical warm trains are ~10 times longer, five times larger and last several times longer than the cold trains. The comparison is summarized in Table 2.

Table 2. Comparison between the "classical" warm trains (see Sec. 1, above) and the trains analyzed here

Characteristic	Typical length (Km)	Size of individual cells (Km)	Time-scale	Main season	Synoptic & Thermal background	Major factor
Classical warm train	Several hundreds	50	Half a day	Warm season	Quasi-stationary cold front Warm tongue	Spontaneous, via buoyancy
Cold trains analyzed here	Less than 100	10	Several hours	Cold season	Cold air mass in occluded cyclone	Forced, left of maximum wind belt, in south margins of a CL

300

The trains analyzed in this study share common features with the coastal fronts related to CLs, studied by Rosenfeld and Nirel (1996) and by Goldreich et al. (2004). Both are found over the southern part of the EM, zonally oriented (parallel to the North African coast). They cross the Israeli coastline and produce continuous, and sometimes heavy, rains, with total rainfall that in some cases exceeds 50 mm. However, several substantial

305 differences can be noted between these two phenomena.

The term 'coastal front' was named by Bozart (1975) for cloud bands that develop over the sea, near and parallel to coastlines, as an outcome of land-sea contrast in temperature or friction. Rosenfeld and Nirel (1996) explained the formation of the coastal fronts as resulting from a convergence band, where the warmer sea generates a land-breeze from Egypt. This breeze blows towards the Mediterranean Sea, and confluents offshore

310 with the nearly geostrophic westerly flow over the warmer sea surface (Fig. 1). They based their explanation on both friction and temperature contrast. Our analysis did not reveal any lower-level temperature land-sea contrast across the North African coast, as is reflected in the temperature map 850 hPa (Fig. 4c) and in 925 hPa (not shown). Moreover, the occurrence of the trains does not show any diurnal maximum during the night and morning hours (Table 1), when the land breeze is most intense. The coastal fronts are located close to the

315 North African coast and are oriented parallel to it (250°-275°). Consequently, they intersect the EM coast within a narrow segment of ~50 Km, between Gaza and Ashdod (Fig. 1). In contrast, the trains' orientation is highly variable, between 240° and 350°, with a standard deviation of 26° (Table 1) and the EM coast segment affected by them is much wider, about 150 Km. This implies that, unlike the coastal fronts, the trains do not owe their existence and location to the north African coast.

320 The coastal fronts differ from the trains also in their frequency and dimensions. The number of coastal fronts observed by Rosenfeld and Nirel (1996) is 6 in 11 winters, reflecting a small frequency compared to the 17 train events identified as 'warm trains' within less than 4 winters in this study. As for the dimensions, the coastal fronts are larger than the trains. Their horizontal dimensions are ~3 times larger, and they last 9 times longer. It can be concluded that in spite of the apparent similarity between the coastal fronts and the trains, both

325 associated with CLs, these are different phenomena.

This research sheds light on a specific source of flash floods: CL induced trains, which hit the coastal region of Israel in the winter. This phenomenon gave us an opportunity to inquire into the inner structure of the wind field associated with the CLs and its dynamic implications. It is suggested that this type of maximum wind belt, with which these trains are associated, is an ingredient of the CL, and that in most of the events it denotes

330 the southern limit of its precipitative region. The results of our study identifies a type of regions that are prone to continuous heavy rains through the wind field. The precision of the regional models in mapping the meso-

scale structure of the wind field enables us to point at the left side of maximum wind bands south of CLs as potential regions for rain inducing flash floods.

355 *Review statement*

References

Alpert, P., Osetinsky I., Ziv, B. and Shafir, H.: A new seasons' definition based on the classified daily synoptic systems: An example for the eastern Mediterranean. Int. J. Climatol, 24, 1013–1021,
360 https://doi.org/10.1002/joc.1036, 2004.

Bosart, L. F.: New England coastal frontogenesis. Quart. J. Roy. Met. Soc., 101, 957-978, https://doi.org/10.1002/qj.49710143016, 1975.

Chappell, C. F.: Quasi-stationary convective events. In: Ray, P.S. (eds) Mesoscale Meteorology and Forecasting. American Meteorological Society, Boston, MA. 289-310,
365 https://link.springer.com/chapter/10.1007/978-1-935704-20-1_13, 1986.

Corfidi, S. F.: Cold pools and MCS propagation: forecasting the motion of downwind-developing MCSs, Weather and Forecasting, 18, 997-1017, https://doi.org/10.1175/1520-0434(2003)018%3C0997:CPAMPF%3E2.0.CO;2, 2003.

Dayan, U., Lensky, I. M., Ziv, B. and Khain, P.: Atmospheric conditions leading to an exceptional fatal flash
370 flood in the Negev Desert, Israel, Natural Hazards Earth Syst., Sci, 21, 1583-1597, https://doi.org/10.5194/nhess-21-1583-2021, 2021.

Doswell III, C. A., 1987: The distinction between large-scale and mesoscale contribution to severe convection: A case study example. Weather Forecast., 2, 3–16, https://doi.org/10.1175/1520-0434(1987)002%3C0003:TDBLSA%3E2.0.CO;2, 1987.

375   Doswell III, C. A., Brooks, H. E. and Maddox, R. A.: Flash flood forecasting: an ingredients-based methodology, Weather Forecast., 11, 560-581, https://doi.org/10.1175/1520-0434(1996)011%3C0560:FFFAIB%3E2.0.CO;2, 1996.

Goldreich, Y., Moses H. and Rosenfeld D.: Radar analysis of cloud systems and their rainfall yield in Israel. Isr. J. Earth Sci. 53, 63–76, DOI:10.1560/G68K-30MN-D5V0-KUHU, 2004.

380   Haiden, T., Kann, A., Wittmann, C., Pistotnik, G., Bica, B., and Gruber, C.: The Integrated nowcasting through comprehensive analysis (INCA) system and its validation over the Eastern Alpine region, Weather Forecast., 26, 166–183, https://doi.org/10.1175/2010WAF2222451.1, 2011.

HMSO: Weather in the Mediterranean I: General Meteorology, 2d ed., Her Majesty's Stationery Office, 362 p., 1962.

385   Hólm, E., Forbes, R., Lang, S., Magnusson, L. and Malardel, S.: New model cycle brings higher resolution, ECMWF Newsletter, issue 147, pp. 14-19. DOI: 10.21957/s2gvuwmg, 2016.

Israel Meteorological Service (IMS) publication: Summary of the rain event in 6-8 December 2018 (in Hebrew) https://ims.gov.il/sites/default/files/2020-09/%D7%A1%D7%99%D7%9B%D7%95%D7%9D%20%D7%90%D7%99%D7%A8%D7%95%D7%A2%20%D7%94%D7%92%D7%A9%D7%9D%208-390   6%20%D7%91%D7%93%D7%A6%D7%9E%D7%91%D7%A8%202018.pdf, 2018

Katsnelson, J.: The variability of annual precipitation in Palestine. Arch. Meteor. Geophys. Biokl. B. 13, 163–172, https://doi.org/10.1007/BF02243250, 1964.

Morin, E., Harats, N., Jacoby, Y., Arbel, S., Getker, M., Arazi, A., Grodek, T., Ziv, B., and Dayan, U.: 395   Studying the extremes: hydrometeorological investigation of a flood causing rainstorm over Israel, Adv. Geosci., 12, 107–114, https://doi.org/10.5194/adgeo-12-107-2007, 2007.

Rigo, T. and Llasat, M. C.: Radar analysis of the life cycle of Mesoscale Convective Systems during the 10 June 2000 event, Nat. Hazards Earth Syst. Sci., 5, 959–970, https://doi.org/10.5194/nhess-5-959-2005, 2005.

400   Rosenfeld D. and Nirel, R.: Seeding effectiveness - the interaction of the desert dust and the southern margins of rain cloud systems in Israel. J. App. Meteor., 35, 1502-1510, https://doi.org/10.1175/1520-0450(1996)035%3C1502:SEIODD%3E2.0.CO;2, 1996.

Saaroni, H., Halfon, N., Ziv, B., Alpert, P. and Kutiel, H.: Links between the rainfall regime in Israel and location and intensity of Cyprus lows, Int. J. Clim., 30, 1014–1025, https://doi.org/10.1002/joc.1912, 2010.

405   Sandler, D., Saaroni, H., Ziv, B., Hochman, A., Harnik, N. and Rostkier-Edelstein, D: A multiscale approach to statistical downscaling of daily precipitation: Israel as a test case, Int. J. Climatol., 44(1), 59-71. https://doi.org/10.1002/joc.8315, 2024.

Schwartz , B. A., Chappell, C. F., Togstad W. E. and Zhong, X. P.: The Minneapolis Flash Flood: Meteorological Analysis and Operational Response, Wea. Forecasting, 5, 1: 3-21, 410   DOI: https://doi.org/10.1175/1520-0434(1990)005<0003:TMFFMA>2.0.CO;2, 1990.

Sinclair, M. R. and Revell, M. J.: Classification and composite diagnosis of extratropical cyclogenesis events in the southwest Pacific. Mon. Weather Rev., 128, 1089–1105. https://doi.org/10.1175/1520-0493(2000)128<1089:CACDOE>2.0.CO;2, 2000.

Striem, H. L.: Properties of rainspells at Jerusalem and some of their implications for the rain-producing 415   process. Isr. Meteor. Res. Papers, 3, 105-118, 1981.

Ulbrich, U., Lionello, P, and Belušić, D. et al.: Climate and the Mediterranean: synoptic patterns, temperature, precipitation, winds and their extremes. In: Lionello P (ed) The climate of the Mediterranean region: from the past to the future. Elsevier, London, pp 301–346, http://dx.doi.org/10.1016/B978-0-12-416042-2.00005-7, 2012.

420   Volken, E.; Brönnimann, S Meteorologische, Zeitschrift (2011). 20 (3): 351–360. Bibcode:2011MetZe..20..351K. doi:10.1127/0941-2948/2011/105

Wang, S., and Chen, T. C.,: The late-spring maximum of rainfall over the U.S. central plains and the role of the low-level jet, J. Climate, 22, 4696-4709, https://doi.org/10.1175/2009JCLI2719.1, 2009.

Young, A., Bhattacharya, B., and Zevenbergen, C.: A rainfall threshold-based approach to early warnings in
425   urban data-scarce regions: A case study of pluvial flooding in Alexandria, Egypt, Egypt. J. Flood Risk Management. 2021, 14:e12702. https://doi.org/10.1111/jfr3.12702, 2021.

ZAMG, Cumulonimbus (Cb) and Mesoscale Convective System (MCS): special investigation: the train effect or train mechanism, https://resources.eumetrain.org/satmanu/CMs/Cb/navmenu.php?page=7.0.0, 2014.